Hindawi Publishing Corporation
Journal of Nanomaterials
Volume 2014, Article ID 171045, 10 pages
http://dx.doi.org/10.1155/2014/171045

Research Article

Behavior of Yb^{3+} and Er^{3+} during Heat Treatment in Oxyfluoride Glass Ceramics

M. H. Imanieh,[1,2] I. R. Martín,[3,4] J. Gonzalez-Platas,[5,6] B. Eftekhari Yekta,[2] V. K. Marghussian,[2] and S. Shakhesi[7]

[1] *Department of Chemical and Environmental Engineering, University of Toledo, Toledo, OH 43606, USA*
[2] *Ceramic Division, Department of Materials, Iran University of Science and Technology, Narmak, Tehran 1684613114, Iran*
[3] *Departamento de Física Fundamental y Experimental, Electrónica y Sistemas, Universidad de La Laguna, Avenida Astrofísico Francisco Sánchez, La Laguna, 38206 Tenerife, Spain*
[4] *MALTA Consolider Team, La Laguna, 38206 Tenerife, Spain*
[5] *Departamento de Física Fundamental II, Tenerife, Spain*
[6] *Servicio Integrado de Difracción de Rayos X, Tenerife, Spain*
[7] *Nanotechnology Department, Engineering Research Institute, Tehran 1465774111, Iran*

Correspondence should be addressed to M. H. Imanieh; mahammad.imanieh@utoledo.edu

Received 7 September 2013; Revised 2 December 2013; Accepted 6 December 2013; Published 2 January 2014

Academic Editor: Mohsen Rahmani

The effects of alumina content and heat treatment on upconversion properties of codoped (ErF_3-YbF_3) oxyfluoride glass ceramics were investigated. Results showed that alumina content had an effect on phase separation and viscosity of the glass. Due to the high viscosity of low alumina content glass, the phase separated areas were smaller in these specimens. Increasing the heat treatment temperature led to the incorporation of Er^{3+} ions into CaF_2 crystals and also increased the Yb^{3+} concentration in them. This increase improved the energy transfer and back transfer process between Er^{3+} and Yb^{3+} ions and as result upconversion intensity was increased.

1. Introduction

At present, there is great interest in luminescent materials for efficient frequency conversion from infrared to visible radiation, mainly because a visible source pumped by a near infrared laser is useful for high-capacity data storage optical devices [1]. This process can be obtained by upconversion mechanisms, where several infrared photons can be absorbed by the material doped with rare earth ions (RE) in order to populate more energetic levels. Therefore, both the fluorescence lifetime and the stimulated emission cross-section of the RE excited level should be maximized, whereas the nonradiative decay mechanisms should be minimized [2].

Oxyfluoride glass ceramics are ambivalent materials. Despite the fact that they are mainly oxide glasses, they can exhibit optical properties of fluoride single crystals when they are doped with rare earth ions. They are often called nanocomposite materials. Their weird character is obtained by a classical melting and quenching preparation in air followed by an adapted thermal treatment during which fluoride phases are crystallized. The size, size distribution, and volume concentration of fluoride crystallites are crucial for photonic applications. For example, to be a promising optical functional material, the size of the crystallites should be smaller than at least half of the wavelength of the light used while the size distribution should be narrow and the crystallites should possess a homogeneous spatial distribution. In this way, according to the scattering theory developed by Rayleigh [3], complete transparency of a light transmitting material can be attained [4]. A refractive index difference between the amorphous and crystalline phases of less than 0.1 is also required. However, according to Beall and Pinckney [5], based on Hopper's model, crystal sizes of 30 nm and differences in refractive index of 0.3 may be acceptable, provided that the crystal spacing is not larger than six times the average crystal size. Transparent Glass Ceramic (TGC) can also be

Table 1: Composition (mol%), fluorine content (Wt%), and characteristic temperatures (T_g, T_m, and crystallization temperatures of CaF_2 and $Ca_2Al_3O_6F$ in ˚C) of the precursor glass samples.

Sample code	SiO_2	Al_2O_3	CaF_2	ErF_3	YbF_3	Fluorine content	T_g/T_m	CaF_2	$Ca_2Al_3O_6F$
SA1.8	45	25	35	—	—	11.5 ± 0.01	583/969	720	867
SA2.18	48	22	35	—	—	11.00 ± 0.01	570/984	705	861
SA1.8EY	45	25	35	0.5	2	12.4 ± 0.01	500, 605/1009	675	871
SA2.18EY	48	22	35	0.5	2	12.2 ± 0.01	461/1018	660	865

obtained with even larger crystal sizes if optical isotropy is achieved within the glass ceramic [6]. Consequently, the selection of the oxide glass composition and the fluoride phase composition is the key factor in obtaining the desired glass ceramic materials [7–9]. The Er^{3+} ions are specially interesting due to their emission at 1.5 μm and the green upconversion obtained under near infrared excitation [10–12]. In order to improve these emissions, the sensitization of this nanocomposite with Yb^{3+} ions may be a good choice because of the efficient energy transfer process from Yb^{3+} to Er^{3+} ions [10, 11].

Recently upconversion luminescence properties of Er^{3+}/Yb^{3+} codoped glass ceramics containing CaF_2 nanocrystals were investigated by Chen et al. [11] and Kishi et al. [13]. In these researches the authors analyzed the infrared and the upconversion fluorescence produced by Er^{3+} and Yb^{3+} ions. In addition, Perez-Rodriguez et al. [14] studied the upconversion emission properties of Er^{3+}-Yb^{3+} codoped glass and glass ceramic samples with different Si/Al ratios were analyzed by covering their surfaces with silica microspheres (3.8 μm diameter). However, it is necessary to analyze the effect of base glass composition on optical properties and crystallization mechanism of oxyfluoride glass ceramics in order to improve their optical properties.

In this paper, two series SiO_2/Al_2O_3 = 2.18 and SiO_2/Al_2O_3 = 1.8 of oxyfluoride glass ceramics containing CaF_2 nanocrystals doped with a fixed amount of Er^{3+} and Yb^{3+} (0.5 mol% ErF_3 and 2 mol% YbF_3) heat treated at four different temperatures (630, 660, 675, and 690˚C) for 48 h were studied in order to improve Er^{3+} emissions. Based on emission spectra and luminescence lifetimes, the behavior of Er^{3+} and Yb^{3+} ions during heat treatment was evaluated.

2. Experimental

Reagent-Grade Chemicals. (opti pure), SiO_2 (Alfa-aesar-89709), Al_2O_3 (Alfa-aesar42571), CaF_2 (MERCK 102840 precipitated pure), ErF_3 (Alfa-aesar 13653), and YbF_3 (Across 31616) were used as raw materials. The batch compositions were mixed in Agate mortar for 10 min in a glove box with the humidity of less than 10%.

The glass samples were prepared by melting the mixtures of the above mentioned materials in covered platinum crucibles at 1450˚C in an electric kiln for 90 min. Four different batches were used in this study and they are coded in Table 1.

In order to measure fluorine loss in as-made glass, one gram (1.0000) sample of the glass is fused with 3 grams of sodium hydroxide in platinum crucible at 900˚C for 60 min. The fused cake is leached with hot water, filtered, and washed several times with hot water. The above solution is stirred for 3 hours at 80˚C temperature. During this time the pH of the solution decreases to 7 by using sulfuric acid with concentration of 1 M. Using ion chromatography the fluorine concentrations of the solutions are calculated and the fluorine loss of the glass is measured subsequently (Table 1).

The prepared glass was annealed at 480˚C (close to the glass transition temperatures) for 3 h. The resulting samples were cut and polished to form 30 mm × 30 mm × 2 mm rectangular slices. Crystallization temperatures of glass were determined by differential thermal analysis (DTA; Polymer Laboratories 1640, Amherst, MA).

Glass frit with relatively coarse particle sizes (0.30–0.4 mm) and a heating rate of 10 K/min were used in each DTA run. This particle size was chosen in order to minimize the contribution of the surface area to the nucleation process and to obtain DTA results that were closer to the bulk glass. The reference material in these experiments was α-Al_2O_3 powder.

The heat treatment of glass was carried out in an electric kiln at four different temperatures (630, 660, 675, and 690˚C) for 48 h according to DTA results, at a heating rate of 10 K/min. The crystalline phases which were precipitated during the heat treatment were identified utilizing Philips X'Pert Pro diffractometer equipped with a primary monochromator, Cu Kα radiation, and a X'Celerator detector. The XRD patterns were collected with a step of 0.016˚ in the 2θ angular range of 10˚ to 90˚ and acquisition time of 2 h. The microstructure of the heat treated samples was obtained by FESEM (Hitachi S4160) microscope. Samples were imaged after polishing (up to 1 μm diamond paste) and etching in a 0.5 volume percent HF solution for 5 min. Moreover, transmission electron microscopy observations were carried out by using TEM, Phillips CM 200, equipped with the EDAX DX4 EDX detector.

A passively tunable Ti:Sapphire laser source (Spectra-Physics 3900S) pumped by a Millenia spectra-physic laser (model 15SJSPG) was used as an excitation source for upconversion luminescence. The upconverted light was recorded by a spectrometer (Ocean Optics HR4000) equipped with optical fiber with 200 μm diameter. In all the measurements the spectral resolution was about 0.5 nm.

The luminescence decay curves of the $^4I_{11/2}$ and $^4S_{3/2}$ levels were measured by exciting the sample with an optical parametric oscillator OPO (EKSPLA/NT342/3UVE) and were recorded and averaged using a digital storage oscilloscope (Tektronix 2430A).

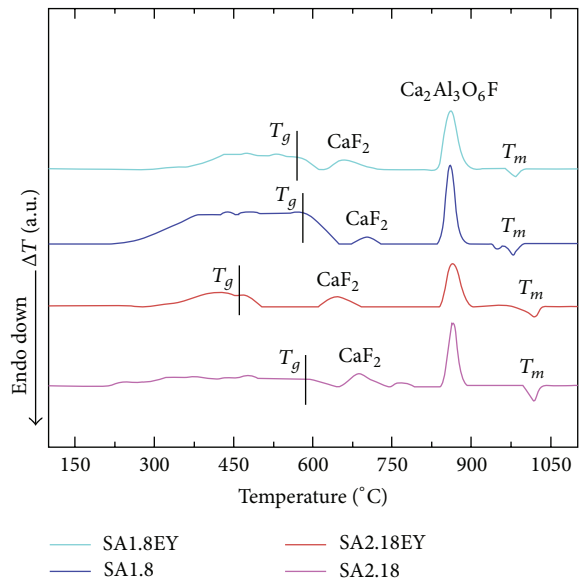

FIGURE 1: DTA thermographs of SA2.18, SA2.18EY, SA1.8, and SA1.8EY glass.

3. Results and Discussion

3.1. DTA Analysis. Figure 1 shows the DTA thermographs of the oxyfluoride glass specimens with the compositions shown in Table 1. The thermal event that arises at the lowest temperature is the glass transition temperature (T_g). As shown, it was followed by two exothermic effects showing the crystallizations of various phases. According to X-ray diffraction results, the first and the second exothermic peaks belong to crystallization of CaF_2 and $Ca_2Al_3O_6F$, respectively. As it can be seen, there is also an endothermic peak in the glass (T_m). XRD results showed that this peak was related to dissolution of fluorine in the residual glass phase. These characteristic temperatures of the glass, that is, T_g, crystallization temperatures, and T_m, have been summarized in Table 1.

According to Chen et al. [7, 15] and Bao et al. [8], Er^{3+} ion could play a significant role in the crystallization of CaF_2 in the oxyfluoride glass. In SA1.8EY, this temperature is reduced from 720°C to 675°C and in SA2.18EY from 705°C to 660°C with the incorporation of these ions.

Although influence of Yb^{3+} in the crystallization of CaF_2 in the oxyfluoride glass is not clear, there are some reports showing that the YbF_3 promotes the crystallization of the fluoride phases such as LaF_3 [16] or PbF_3 [17]. Further works in single doped samples with Yb^{3+} indicate that this ion does not act as nucleating agent for CaF_2 in SiO_2-Al_2O_3-CaF_2 system [18].

According to Hill et al. [19], in oxyfluoride glass, the fluorine was bonded to the aluminum ions which were present in the glass composition. As a result of this, there was less fluorine loss due to lower silicon tetrafluoride (SiF_4) formation [20]. It seems that a similar situation could happen in glass under study. As it can be seen from Table 1, increasing the alumina content resulted in the decrease of the fluorine loss during the melting. Owing to higher concentration of the fluorine bond in the SA1.8 doped glass the dissolution of fluorine (T_m) takes place in a lower temperature than the other ratio (see Table 1).

3.2. Microstructural Evaluation. The SEM images (Figures 2(a) and 2(b)) of samples SA2.18EY and SA1.8EY after heat treatment at 590°C for 10 minutes with ramp rate of 10 K/min revealed that large separation areas (droplets) were formed in the SA1.8EY samples in comparison to the SA2.18EY samples. Phase separation in oxyfluoride glass ceramic is a common phenomenon [4, 21]. It is very likely that the described samples are phase separated; because rare earth ions are known to introduce phase separation droplets into the glass already in minor concentrations [18, 21].

According to DTA results, the crystallization of CaF_2 in the glass with higher alumina content and lower viscosity took place at higher temperatures than the other ones. Low viscosity promotes the occurrence of phase separation in glass, and, as a result of this, large separation areas (droplets) were formed in the SA1.8EY samples in comparison with the SA2.18EY samples. As the separated areas are smaller in the SA2.18EY specimens, the concentration of CaF_2 will be increased locally and the crystallization temperature of CaF_2 would be decreased more than the samples of the other ratio. Similar behavior was suggested in SiO_2-Al_2O_3-Na_2O-LaF_3 system by Bhattacharyya et al. [4].

A bright field and dark field transmission electron microscopy images of the glass ceramics SA1.8EY heat-treated at 675°C for 48 hours are shown in Figures 3(a) and 3(b), respectively. One can see in the bright field image the two phases of the glass ceramic: the black spots correspond to the crystallites in diffraction conditions and the white background corresponds to the glassy matrix. Lots of spherical CaF_2 crystallites sized about 20–60 nm are distributed separately among the glassy matrix. Their corresponding electron diffraction pattern is shown in the inset of Figure 3(a). The average size calculated by analyzing many TEM images is 35 ± 10 nm.

3.3. X-Ray Diffraction Analysis. Figures 4(a) and 4(b) show XRD patterns of SA1.8EY and SA2.18EY samples which were heat treated at 630, 660, 675, and 690°C for 48 h.

Several diffraction peaks corresponding to CaF_2 (ICCD no. 00-002-1302) crystals are clearly observed in the mentioned samples, indicating the crystallization of CaF_2 crystals in the precursor glass. The diameters of the crystals in the samples were evaluated by the Scherrer formula, and they are given in Figure 5. Due to the smaller size of precipitated CaF_2 crystals in the SA2.18EY samples than SA1.8EY, these samples maintained excellent transparency.

According to XRD patterns, the volume fraction of the crystal phase can be approximately estimated by the ratio of the integrated area of the peaks with respect to the total XRD patterns. All calculated data is plotted in Figure 5, and as seen the crystal size was risen with an increase in heat treatment temperature from 630 to 690°C (from 8.5 nm to 22 nm in SA2.18EY and from 20 nm to 34 nm SA1.8EY sample). As Chen et al. mentioned, the crystallization of CaF_2 in oxyfluoride glass ceramic is a diffusion-controlled process

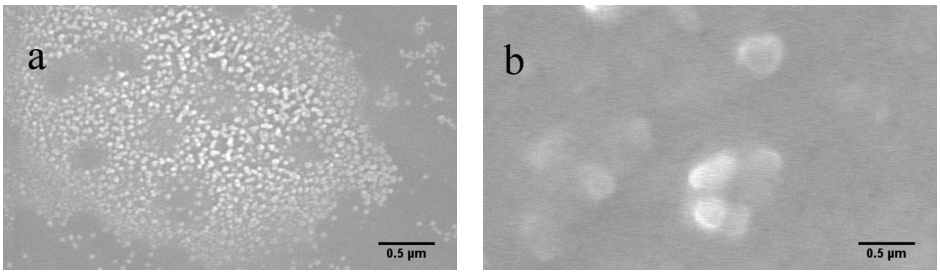

(a) (b)

Figure 2: SEM images of samples (a) SA2.18 EY and (b) SA1.8 EY after heat treatment at 590°C for 10 min.

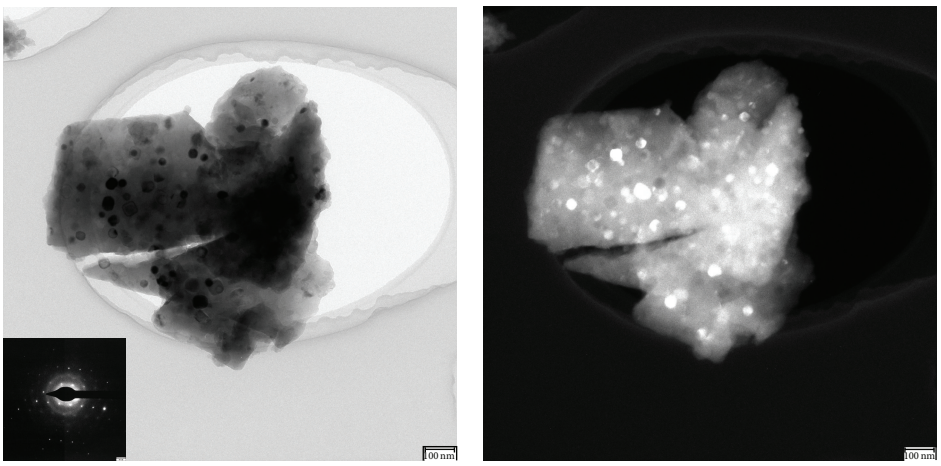

(a) (b)

Figure 3: TEM images of (a) bright field and (b) dark field of the SA1.8EY sample heat treated at 675°C for 48 hours. The inset in (a) shows the corresponding electron diffraction pattern.

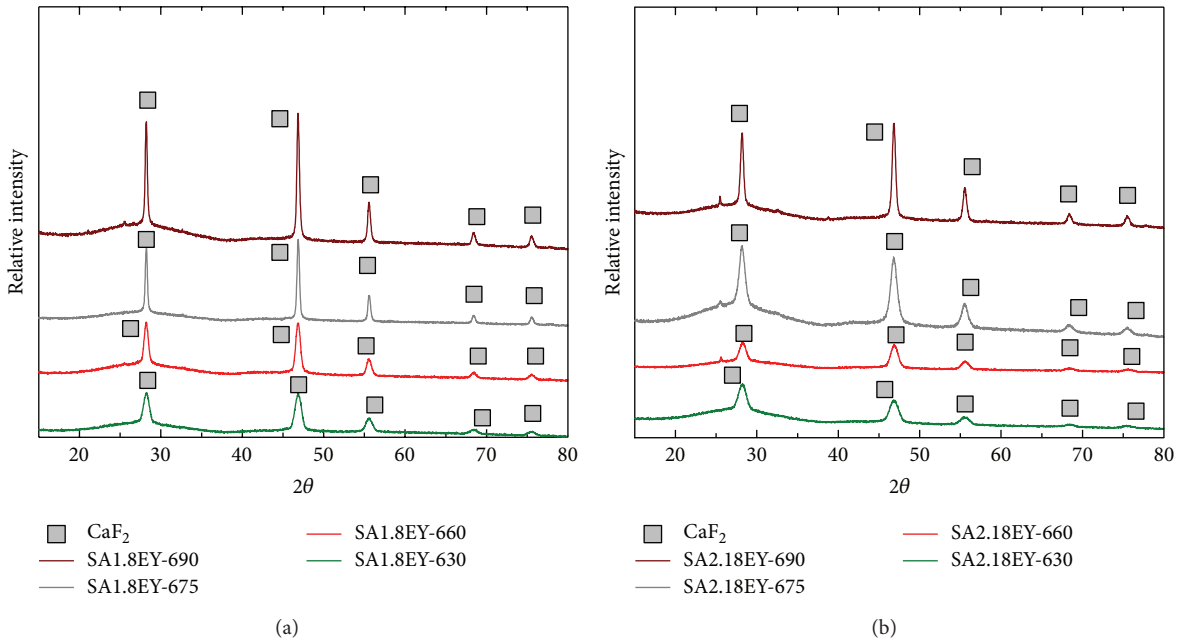

(a) (b)

Figure 4: XRD patterns of (a) SA1.8EY and (b) SA2.18EY samples which were heat treated at 630, 660, 675, and 690°C for 48 hours.

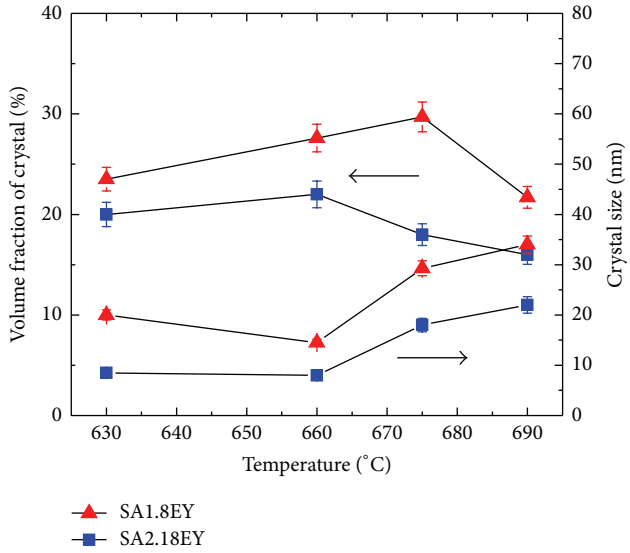

FIGURE 5: Crystal size and volume fraction of CaF_2 crystallites in SA1.8EY and SA2.18EY samples heat treated at different temperatures.

[7]. According to this mechanism, the local composition changes during crystallization, and the crystal growth rate depends exponentially on the heating temperature.

The volume concentration of crystalline CaF_2 in each ratio reaches a maximum and decreases afterward. This maximum is 22% for SA2.18EY at 660°C and 30% for SA1.8EY at 675°C. These two temperatures correspond to the maximum of CaF_2 crystallization temperature due to DTA results for each sample. At this temperature, the nucleation and growth of nucleus have the same rate as other temperatures. As a result, more nuclei were formed at the maximum of the crystallization peak, and volume concentration of CaF_2 was increased at this temperature as well. Russel [22] suggested a mechanism for the crystallization of CaF_2 in aluminosilicate glass, in which the interface is enriched in glass formers, increasing the viscosity near the crystals. Thus, a diffusional barrier around each crystal is formed, which hinders further crystal growth [22].

Although Russell did not mention the occurrence of phase separation in their glass, as mentioned before, our samples were phase separated. However, Russell studied different glass compositions located in the Na_2O-K_2O-CaO-CaF_2-Al_2O_3-SiO_2 system, and it is possible that their glass did not undergo phase separation.

Therefore, there are two parameters which could control the crystal size and size distribution, namely, the phase separated droplet size and the diffusional barrier around each crystal in phase separated droplet. These parameters are both controlled by the viscosity of glass.

Upon subsequent heat treatment, while the CaF_2 nanocrystals are formed within these phase separated droplets, SiO_2, also contained in the phase separated droplets, is relocated to the periphery of the droplets, hence inhibiting further crystal growth [4, 22].

In SA2.18EY with lower alumina content, the viscosity of the glass is higher than the other one (SA1.8EY); hence the phase separated droplets are smaller. Additionally, due to the existence of higher viscosity, the diffusional barrier formed faster, and further nucleation became more and more difficult. Therefore, the size and concentration of crystalline CaF_2 are smaller than the other ratio.

3.4. Direct Excitation and Upconversion. Figure 6 shows the upconversion luminescence of samples which were heat treated at 630, 660, 675, and 690°C for 48 h and excited by 975 nm. The emission bands of the Er^{3+} ions can be assigned to the $^2H_{11/2} \rightarrow {}^4I_{15/2}$ (520 nm), $^4S_{3/2} \rightarrow {}^4I_{15/2}$ (545 nm), and $^4F_{9/2} \rightarrow {}^4I_{15/2}$ (660 nm) transitions, respectively. As can be observed, in general the upconversion luminescence emission intensity increased with rising heat treatment temperature. Moreover, in these heat treated samples, the upconversion emission shows bands with well resolved structure, confirming again the incorporation of Er^{3+} ions into the nanocrystals. It is well known that the upconversion luminescence of rare earth ions is affected by multiphonon relaxation.

According to the Miyakawa and Dexter theory [23], the multiphonon decay rate depends exponentially on the energy gap to the next lower level and on the energy of the maximum lattice vibration of the surrounding host lattice [23]. The approximate frequency of the highest energy lattice vibration in silicate oxide glass is 1100 cm^{-1}, and this value decreases to 280 cm^{-1} for a CaF_2 crystal. As mentioned before, increasing the heat treatment time and temperature leads to incorporation of Er^{3+} ions into CaF_2 crystalline phase. Therefore, the upconversion intensity is increased significantly due to the decrease of the multiphonon relaxation with the increase of heat treatment time and temperature. For this reason, the upconversion emission obtained from the glass ceramic samples is much higher than the precursor glass (see Figure 6).

Moreover, comparing the results shown in Figure 6, it can be seen that the intensity of upconversion is higher in the SA2.18 than SA1.8 samples. This is due to the smaller crystal size of CaF_2 in this ratio. It seems that in the SA2.18EY matrix the distance between Er^{3+} and Yb^{3+} ions is shorter, and as result there is more energy transfer between them. Having more energy transfer processes between Er^{3+} and Yb^{3+} ions resulted in increasing the upconversion luminescence.

As Er^{3+} ions act as nucleate agents for CaF_2 crystals [7], during the heat treatment Er^{3+} ions are incorporated in the CaF_2 crystals at the beginning of the formation of the CaF_2 crystals. On the other hand, Yb^{3+} ions remain in the glass phase. As mentioned before, the crystal size was risen with increasing the heat treatment temperature. As a result, there are more Yb^{3+} ions near the surface of the crystals. According to phase diagram of the CaF_2-YbF_3 system [11], CaF_2 and YbF_3 yield a solid solution in the range of about 0–35 mol% YbF_3 content [11]. Therefore, the Yb^{3+} ions are considered to be incorporated into the CaF_2 to form $(Ca_{1-x}\ Yb_x)F_{2+x}$ solid-solution crystals during the heat treatment of the samples.

In Figure 7, the relative intensity of the green and red emission in upconversion (Figure 7) can be seen. In order to

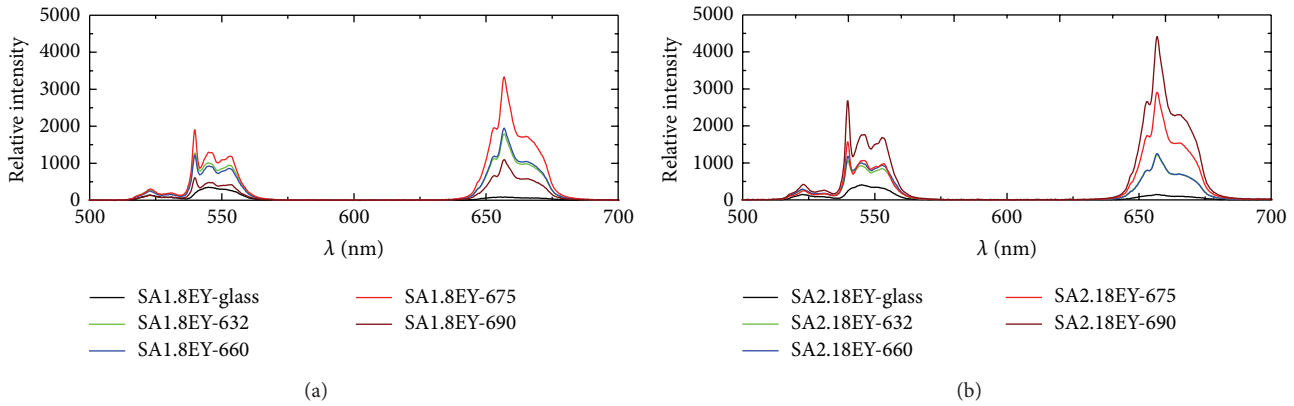

FIGURE 6: Upconversion luminescence in SA1.8EY and A2.18EY samples that obtained exciting at 975 nm which were heat treated at 630, 660, 675, and 690°C for 48 h.

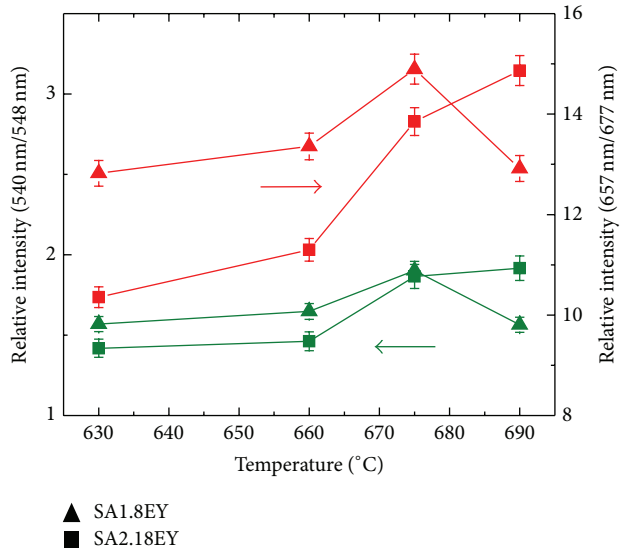

FIGURE 7: Relative intensity of the green (green symbols) and red (red symbols) upconversion bands that obtained exciting at 975 nm.

calculate this relative intensity, the wavelengths with highest (540 nm and 657 nm) and lowest (548 nm and 677) intensity with respect to the glass intensity are chosen. These ratios will predominantly proportion the intensity of the emission coming from ions inside the nanocrystals with respect to the ions inside the glassy phase.

According to the results shown in Figure 7, increasing the temperature of the heat treatment leads to a rise in the red and green emissions in the upconversion luminescence of the samples in SA2.18EY ratio. On the other hand, in SA1.8EY ratio there is an increase in the relative red and green emissions until 675°C and the decrease after the heat treatment temperature reaches 690°C.

3.5. Fluorescence Decay Analysis. The fluorescence decays of Er^{3+} ions in the samples around 842 nm, which correspond to the $^4S_{3/2} \rightarrow {}^4I_{13/2}$ transition, are shown in Figure 8. These decays were obtained under pulse excitation of the $^4S_{3/2}$ level at 550 nm. In this figure, it can be seen that the lifetime of the Er^{3+} ions increases slightly with the heat treatment temperature in the SA1.8EY ratio. Probably, after crystallization of CaF_2 in the glass, the majority of Er^{3+} ions are incorporated in the CaF_2 crystals. As it was mentioned before, the multiphonon decay rate decreases in the ions inside the CaF_2 nanocrystals. As a result, the ions inside the nano-crystal have a longer lifetime. Further temperature increases to 690°C leading a rise in the Er^{3+} concentration in the CaF_2 crystals and thus improving the energy transfer between Er^{3+} ions. This then leads to most of the excited energy states going to the ground state by means of transfer to traps or cross-relaxation process, leading to the concentration quenching. Similar behavior was reported by Yan et al. in $SrAl_{12}O_{19}$ nanophosphors [24]. Therefore, the lifetime at 690°C is shorter than the other samples (Figure 8), and it could also explain the decreasing of the relative green and red emission intensity obtained in the Figure 7.

On the other hand, in SA2.18EY the lifetime of the Er^{3+} ions increased slightly with the heat treatment temperature. Due to high viscosity of the glass in this ratio, the ions have less mobility than the other ratio and as a result the greater part of the Er^{3+} ions remain in the glass phase. Raising the heat treatment temperature (675 and 690°C) leads to increasing the crystal size and the ion diffusion rate; therefore there is more possibility to have Er^{3+} ions inside or on the surface of the CaF_2 crystals. Considering this effect, there are more Er^{3+} ions in the fluoride phase and as a result the lifetime will be increased (see Figure 8). With respect to the other ratio (SA1.8), the concentration of the Er^{3+} ions is lower and these ions can be regarded as isolated and only a few of them with traps nearby can transfer their energy to the traps or undergo the cross-relaxation process, leading to an insignificant concentration quenching. In this case the green and red emission intensity will be increased (see Figure 7).

In order to identify the Yb^{3+} position (glass or crystal phase), the infrared fluorescence decays of the samples around 975 nm were also measured. These decays were obtained under pulse excitation of the $^2F_{5/2}$ level of Yb^{3+} ions

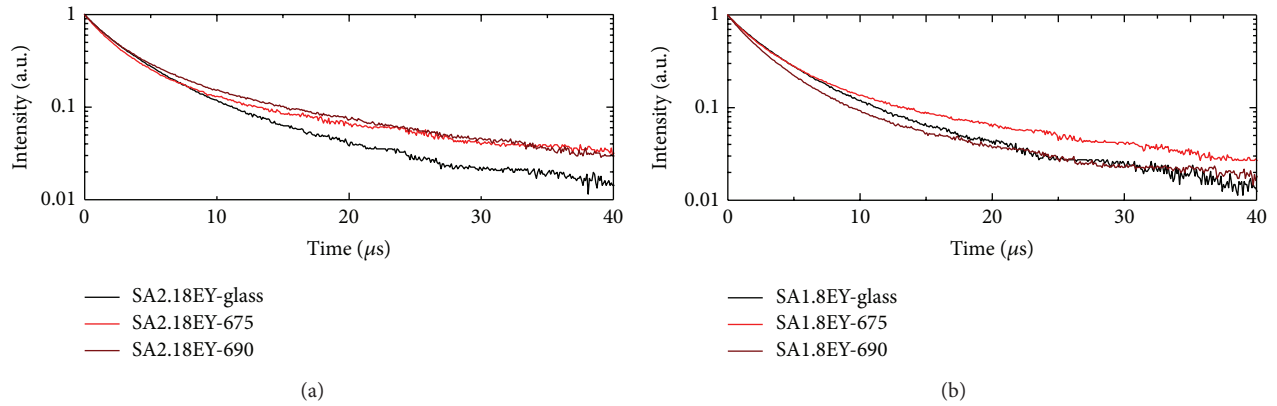

FIGURE 8: Fluorescence decays of Er^{3+} around 842 nm (corresponding to the $^4S_{3/2} \rightarrow {}^4I_{11/2}$ emission) obtained in SA1.8EY and SA2.18EY glass and in these samples heat treated at 675 and 690°C for 48 h and excited at 550 nm.

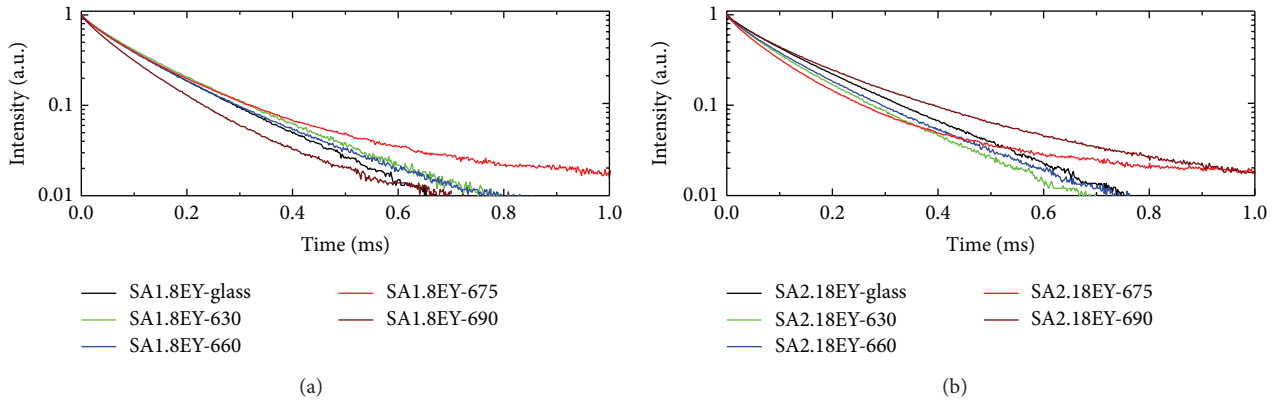

FIGURE 9: Infrared fluorescence decays of the glass around 975 nm in both ratios (SA1.8EY and SA2.18EY) samples which were heat treated at 630, 660, 675, and 690°C for 48 h and excited at 940 nm.

at 940 nm. At 975 nm the Er^{3+} ions have an excited level $^4I_{11/2}$ which coincides with the $^2F_{5/2}$ level of Yb^{3+} ions. Therefore, if transfer and back transfer processes between these ions are important it should be reflected in the experimental decays curves. As an example, in fluoroindate glass these processes were analyzed on basis of the fluorescence transfer function model [10]. As it can be seen from Figure 9, the decay curves of the glass in both ratios indicate that the Yb^{3+} lifetimes are similar.

Comparing the decay curves of the glass and the samples which are heat treated at 630, 660, and 675°C in SA1.8EY and SA2.18EY ratio, it can be concluded that in the glass with higher alumina content (SA1.8EY) and low viscosity the Yb^{3+} ions start to be incorporated into fluoride phase while the heat treatment temperature is rising. Due to transfer and back transfer between Er^{3+} and Yb^{3+} ions inside the low energy phonon fluoride phase the decay time is increased in these samples (Figure 9).

On the other hand, in the glass with lower alumina content (SA2.18EY) and high viscosity, it seems that the majority of Yb^{3+} ions remain inside the glass phase. This can be explained by the diminution of their lifetimes, probably after crystallization of CaF_2 in the glass; as the fluorine content of the glass was reduced, the lifetime of the ions inside the glass would be decreased due to the increase of energy phonon of the glass. As mentioned before rising the temperature to 675°C leads to increasing the size of the nanocrystals and as a result some Yb^{3+} ions are incorporated on the surface of the CaF_2 crystals in SA2.18EY. In this case there will be two groups of Yb^{3+} ions inside the sample, one located on the surface of the nanocrystals and the other one inside the glassy phase. The decay curve of SA2.18EY treated at 675°C which is shown in Figure 9 confirms this result. This curve consists of a short and a long component. The short component is due to the Yb^{3+} ions inside the glass while the long component is related to Yb^{3+} ions on the surface of the CaF_2 nanocrystals. Furthermore in SA1.8EY at 690°C there is a decrease in the lifetime which could be explained on a basis of the concentration quenching. As mentioned before the Er^{3+} concentration in the CaF_2 nanocrystals in this sample is high. Moreover, high concentrations of Yb^{3+} ions were expected in this ratio. As a result, transfer and back transfer among these ions could be very efficient until the energy is transferred to traps. According to this transfer, a decrease

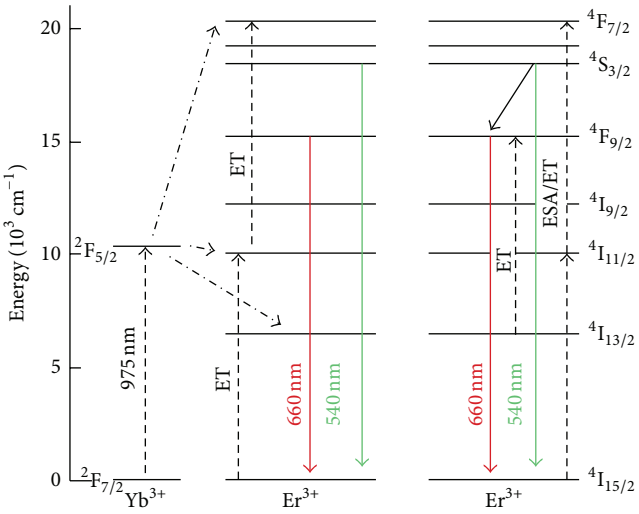

FIGURE 10: Energy-level diagram of Yb^{3+} and Er^{3+} ions and possible upconversion mechanisms.

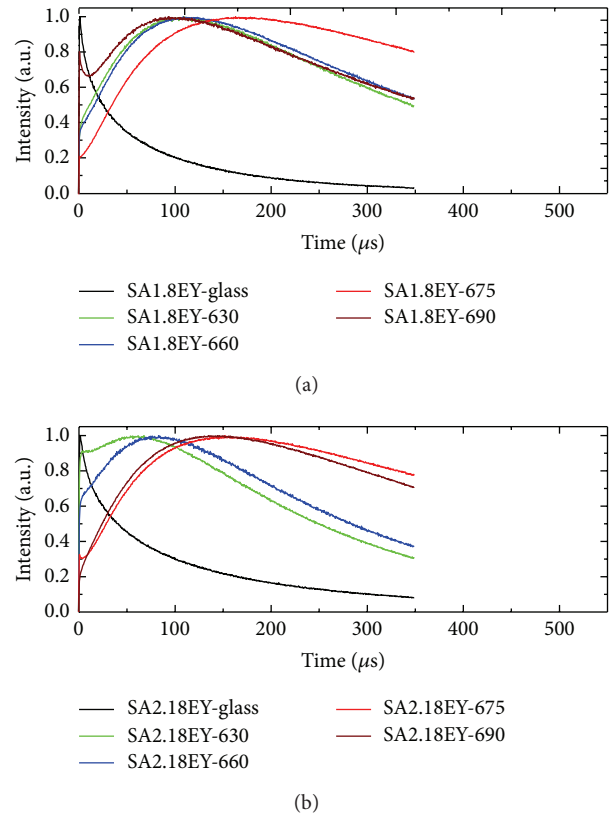

FIGURE 11: Temporal evolution of the upconversion emission at 660 nm with obtained exciting at 975 nm for SA1.8EY and SA2.18EY samples heat treated at 630, 660, 675, and 690°C for 48 h.

in the lifetime is predictable for the SA1.8EY sample at this temperature (as shown in Figure 9).

All processes explained before give to place that the upconversion intensity of the SA2.18EY sample which is heat treated at 690°C for 48 hr should have the highest intensity among the others.

In Figure 10, different upconversion mechanisms to populate the $^4S_{3/2}$ and the $^4F_{9/2}$ emitting levels of Er^{3+} ions under excitation at 975 nm are shown. As it can be seen, the green emitting level ($^4S_{3/2}$) could be populated under excited state absorption (ESA) or energy transfer processes (ET) from the $^4I_{11/2}$ level. Moreover, the $^4F_{9/2}$ level could be populated from relaxation of the $^4S_{3/2}$ level or from an additional upconversion mechanism from the $^4I_{13/2}$ level. Additionally, Yb^{3+} ions in the composition introduce an additional possible mechanism to populate the $^4F_{9/2}$ level of the Er^{3+} ions. This will take place by an extra upconversion processes [25].

With the increase of Yb^{3+} doping content, the electron population of Er^{3+} ions in $^4I_{13/2}$ level is largely increased due to energy transfer from Yb^{3+} to Er^{3+} [7]. Besides, the excited Yb^{3+} ions can produce successive transfer processes in order to excite the Er^{3+} ions to the higher levels (as it is shown in Figure 10). As a result, the enhancement of the red emission will be achieved (as shown in Figure 6).

In Figure 11 the temporal evolution of the red emission under pulsed excitation at 975 nm is shown. In the glass samples the Er^{3+} and Yb^{3+} ions are placed far from each other in random positions of the glass matrix. As result, energy transfer processes between them are negligible. As it can be seen from Figure 11, the emission intensity coming from the ions inside the glass reaches the maximum, immediately after the pump laser. This is related to ESA mechanism which takes place in isolated Er^{3+} ions in the glass matrix in both ratios. As pointed out before, increasing the heat treatment temperature rises the Er^{3+} and Yb^{3+} concentration in the CaF_2 nanocrystals. Decreasing the distance between Er^{3+} ions in the CaF_2 nanocrystals lets additional ET mechanism to excite the $^4F_{9/2}$ level. In this case, the ESA is less important than ET mechanism, which is characterized by a rise in time (as it can be seen in some curves in Figure 11). Comparing the temporal curves of the glass heat treated at 630, 660, and 675°C in the two ratios, it can be concluded that in the SA1.8EY the ET mechanism is activated faster than the SA2.18EY. This is due to higher mobility of ions in this ratio, while in the other ratio the mobility of ions is lower and as a result there is an important difference in ion concentration inside the nanocrystals at different temperatures.

At 675 and 690°C the possibility of having Yb^{3+} ions in the CaF_2 nanocrystals increased. Therefore the ET mechanism will be more important in these temperatures as well.

In SA1.8EY, due to low viscosity of the glass, the ions have higher mobility than the other ratio and as a result the greater part of the Er^{3+} ions are incorporated into nanocrystals. Thus, at 690°C the concentration of both Yb^{3+} and Er^{3+} ions increased. Therefore, as it was obtained previously the quenching processes of the Er^{3+} ions in the nanocrystals produce an important reduction of the emission coming from these ions. As a result, the emission coming from ions excited by ESA mechanism will predominate again to populate the $^4F_{9/2}$ level.

4. Conclusions

The effects of alumina content and heat treatment on upconversion properties of codoped Er^{3+} and Yb^{3+} ions in oxyfluoride glass ceramics were investigated. Results showed that alumina content had a significant effect on phase separation and viscosity of the glass. Due to the high viscosity of low alumina content glass, the phase separated areas were smaller in these specimens. Although the crystallization of CaF_2 took place at lower temperature in this case, it will be frozen faster as well. Due to high viscosity of the glass in this ratio (SA2.18EY) ions have less mobility than the other ratio (SA1.8EY) and as a result the greater part of the Er^{3+} ions remain in the glass phase during the heat treatment process. Also Yb^{3+} ions start to be incorporated into CaF_2 nanocrystals at higher temperature in low alumina content glass (SA2.18EY). These conclusions have been obtained in basis of the analysis of the decay curves for the emission of Er^{3+} at 842 nm and the $Yb^{3+}$and Er^{3+} at 975 nm.

Conflict of Interests

The authors declare that there is no conflict of interests regarding the publication of this paper.

Acknowledgments

The authors thank Ministerio de Economía y Competitividad of Spain (MINECO) within The National Program of Materials (MAT2010-21270-C04-02/-03/-04), the Consolider-Ingenio 2010 Program (MALTA CSD2007-0045, http://www.malta-consolider.com), the EU-FEDER for their financial support, and ACIISI of Gobierno de Canarias for the project ID20100152 and FPI. The authors also thank the Governments of Spain and India for the award of a Project within the Indo-Spanish Joint Programme of Cooperation in Science and Technology (PRI-PIBIN-2011-1153/DST-INT-Spain-P-38-11).

References

[1] M. A. Hernández-Rodríguez, M. H. Imanieh, L. L. Martín, and I. R. Martína, "Experimental enhancement of the photocurrent in a solar cell using upconversion process in fluoroindate glasses exciting at 1480 nm," *Solar Energy Materials and Solar Cells*, vol. 116, pp. 171–175, 2013.

[2] A. Tressaud, *Synthesis, Characterization & Properties of Nanostructured Solids*, vol. 1, John Wiley & Sons, Paris, France, 2010.

[3] L. Rayleigh, "The incidence of light upon a transparent sphere of dimensions comparable with the wave-length," *Proceedings of the Royal Society of London Series A*, vol. 84, no. 567, pp. 25–46, 1910.

[4] S. Bhattacharyya, T. Höche, N. Hemono, M. J. Pascual, and P. A. van Aken, "Nano-crystallization in LaF_3-Na_2O-Al_2O_3-SiO_2 glass," *Journal of Crystal Growth*, vol. 311, no. 18, pp. 4350–4355, 2009.

[5] G. H. Beall and L. R. Pinckney, "Nanophase glass-ceramics," *Journal of the American Ceramic Society*, vol. 82, no. 1, pp. 5–16, 1999.

[6] M. C. Gonçalves, L. F. Santos, and R. M. Almeida, "Rare-earth-doped transparent glass ceramics," *Comptes Rendus Chimie*, vol. 5, no. 12, pp. 845–854, 2002.

[7] D. Chen, Y. Wang, Y. Yu et al., "Influences of Er^{3+} content on structure and upconversion emission of oxyfluoride glass ceramics containing CaF_2 nanocrystals," *Materials Chemistry and Physics*, vol. 95, no. 2-3, pp. 264–269, 2006.

[8] F. Bao, Y. Wang, and Z. Hu, "Influence of Er^{3+} doping on microstructure of oxyfluoride glass-ceramics," *Materials Research Bulletin*, vol. 40, no. 10, pp. 1645–1653, 2005.

[9] M. H. Imanieh et al., "Crystallization of nano calcium fluoride in CaF_2-Al_2O_3-SiO_2 system," *Solid State Sciences*, vol. 17, pp. 76–82, 2013.

[10] I. R. Martin, V. D. Rodríguez, V. Lavín, and U. R. Rodríguez-Mendoza, "Transfer and back transfer processes in Yb^{3+}-Er^{3+} codoped fluoroindate glasses," *Journal of Applied Physics*, vol. 86, no. 2, pp. 935–939, 1999.

[11] D. Chen, Y. Wang, E. Ma, Y. Yu, and F. Liu, "Partition, luminescence and energy transfer of Er^{3+}/Yb^{3+} ions in oxyfluoride glass ceramic containing CaF_2 nano-crystals," *Optical Materials*, vol. 29, no. 12, pp. 1693–1699, 2007.

[12] M. H. Imanieh et al., "Effect of alumina content and heat treatment on microstructure and upconversion emission of Er^{3+} ions in oxyfluoride glass-ceramics," *Journal of Rare Earths*, vol. 30, no. 12, pp. 1228–1234, 2012.

[13] Y. Kishi, S. Tanabe, S. Tochino, and G. Pezzotti, "Fabrication and efficient infrared-to-visible upconversion in transparent glass ceramics of Er-Yb Co-doped CaF_2 nano-crystals," *Journal of the American Ceramic Society*, vol. 88, no. 12, pp. 3423–3426, 2005.

[14] C. Perez-Rodriguez, M. H. Imanieh, L. L. Martín, S. Rios, I. R. Martín, and B. E. Yekta, "Study of the focusing effect of silica microspheres on the upconversion of Er^{3+}-Yb^{3+} codoped glass ceramics," *Journal of Alloys and Compounds*, vol. 576, pp. 363–368, 2013.

[15] D. Chen, Y. Wang, Y. Yu, and E. Ma, "Improvement of Er^{3+} emissions in oxyfluoride glass ceramic nano-composite by thermal treatment," *Journal of Solid State Chemistry*, vol. 179, no. 5, pp. 1445–1452, 2006.

[16] D. Chen, Y. Wang, Y. Yu, and E. Ma, "Influence of Yb^{3+} content on microstructure and fluorescence of oxyfluoride glass ceramics containing LaF_3 nano-crystals," *Materials Chemistry and Physics*, vol. 101, no. 2-3, pp. 464–469, 2007.

[17] G. Dantelle, M. Mortier, D. Vivien, and G. Patriarche, "Nucleation efficiency of erbium and ytterbium fluorides in transparent oxyfluoride glass-ceramics," *Journal of Materials Research*, vol. 20, no. 2, pp. 472–481, 2005.

[18] M. H. Imanieh et al., "Improved cooperative emission in ytterbium-doped oxyfluoride glass-ceramics containing CaF_2 nanocrystals," *Journal of the American Ceramic Society*, vol. 95, no. 12, pp. 3827–3833, 2012.

[19] R. Hill, D. Wood, and M. Thomas, "Trimethylsilylation analysis of the silicate structure of fluoro-alumino-silicate glasses and the structural role of fluorine," *Journal of Materials Science*, vol. 34, no. 8, pp. 1767–1774, 1999.

[20] L. Lin, G. Ren, M. Chen, Y. Liu, and Q. Yang, "Study of fluorine losses and spectroscopic properties of Er^{3+} doped oxyfluoride silicate glasses and glass ceramics," *Optical Materials*, vol. 31, no. 10, pp. 1439–1442, 2009.

[21] N. Hémono, G. Pierre, F. Muñoz, A. de Pablos-Martín, M. J. Pascual, and A. Durán, "Processing of transparent glass-ceramics by nanocrystallisation of LaF_3," *Journal of the European Ceramic Society*, vol. 29, no. 14, pp. 2915–2920, 2009.

[22] C. Russel, "Nanocrystallization of CaF_2 from $Na_2O/K_2O/CaO/CaF_2/Al_2O_3/SiO_2$ glasses," *Chemistry of Materials*, vol. 17, no. 23, pp. 5843–5847, 2005.

[23] T. Miyakawa and D. L. Dexter, "Phonon sidebands, multiphonon relaxation of excited states, and phonon-assisted energy transfer between ions in solids," *Physical Review B*, vol. 1, no. 7, pp. 2961–2969, 1970.

[24] W. Yan, Y. Chen, and M. Yin, "Quenching mechanism of Er^{3+} emissions in Er^{3+}- and Er^{3+}/Yb^{3+}-doped $SrAl_{12}O_{19}$ nanophosphors," *Journal of Rare Earths*, vol. 29, no. 3, pp. 202–206, 2011.

[25] J. del-Castillo, A. C. Yanes, J. Méndez-Ramos, V. K. Tikhomirov, and V. D. Rodríguez, "Structure and up-conversion luminescence in sol-gel derived Er^{3+}-Yb^{3+} co-doped SiO_2:PbF_2 nano-glass-ceramics," *Optical Materials*, vol. 32, no. 1, pp. 104–107, 2009.